npj | 2D Materials and Applications

www.nature.com/npj2dmaterials

ARTICLE OPEN

Check for updates

Exciton dynamics in monolayer graphene grown on a Cu(111) surface

Youngsin Park[1]✉, Guanhua Ying[2], Robert A. Taylor[2] and Chan C. Hwang[3]✉

We have characterized the carrier dynamics of the excitonic emission emerging from a monolayer of graphene grown on a Cu(111) surface. Excitonic emission from the graphene, with strong and sharp peaks both with a full-width at half-maximum of 2.7 meV, was observed near ~3.16 and ~3.18 eV at 4.2 K. The carrier recombination parameters were studied by measuring both temperature-dependent and time-resolved photoluminescence. The intensity variation with temperature of these two peaks shows an opposing trend. The time-resolved emission was modelled using coupled differential equations and the decay time was found to be dominated by carrier trapping and Auger recombination as the temperature increased.

npj 2D Materials and Applications (2021)5:69 ; https://doi.org/10.1038/s41699-021-00252-x

INTRODUCTION

Graphene is an excellent material for fundamental solid-state physics and applications in electronic devices arising from its unique X-band (Dirac cone) energy dispersion, however, it is unsuitable for optical devices based on luminescence because of its zero band gap[1–3] such that optical luminescence is not expected. As excited electrons in the conduction band are easily screened by free electrons in metals, the luminescence efficiency is very low, such that only band to band transitions are significant, as observed in noble metals[4]. Nevertheless, proof-of-concept photonic devices have been demonstrated as photo-detectors[5–8], modulators[9,10], frequency multipliers[11] and mechanical oscillators[12]. As the electronic state is directly related to both optical and transport properties, most research has been focused on the electronic band structure near the Fermi level. For these reasons, measuring photoluminescence (PL) from pristine graphene itself should not be possible unless assisted by phonons introducing confinement such as in graphene quantum dots (GQDs)[13–17] or functionalizing as with graphene oxide (GO)[18–21]. However, many GQDs and GO are not actually pure graphene and the PL peaks from these systems exhibit a broad emission due to the size distribution of the GQDs and inhomogeneities in the oxidation of GO, resulting in unclear transition mechanisms. However, no PL was observed from graphene nanoribbons prepared on metallic substrates due to quenching by the metal[22]. Though the observation of PL has been reported in GQDs[13–17] and GNRs[23–26], all the emission originates from band gap opening. If the band gap of graphene is opened, however, the mobility decreases rapidly due to the inverse relation between the mobility and band gap[27]. So, observing PL from pure graphene whilst keeping its X-band plays a key role in optical devices with high-speed performance. If we can get a sharp and strong luminescence from graphene itself, keeping the X-band structure, nanostructure fabrication such as nanoribbons, GQDs by functionalizing the graphene, is not necessary. Up to now, due to the absence of sharp excitonic emission from the pure graphene, it has been difficult to study optical carrier dynamics experimentally.

Here we discuss excitonic PL dynamics from very sharp and strong peaks at 3.162 and 3.183 eV emerging from pure graphene. Temperature-dependent PL shows that the intensity of these two peaks shows an opposing trend, that is, the intensity of the 3.183 eV peak decreases linearly with increasing temperature whereas that of the 3.162 eV peak increases up to ~45 K and then decreases rapidly. Time-dependent PL measurements show that these two peaks are coupled to each other, compensating the total intensity. The carrier recombination parameters were studied by measuring time-resolved PL (TRPL) and analysed by coupled differential equations.

RESULT AND DISCUSSION

Micro-photoluminescence (μPL)

Several emissions with different origins were observed at low temperature from the pure graphene grown on a Cu(111) surface and a temperature-dependent μPL mapping is shown in Fig. 1a. Very strong and sharp PL peaks both with a full-width at half-maximum (FWHM) of 2.7 meV at 3.162 eV (the lowest emission peak, denoted as P1) and 3.183 eV (denoted as P2) were the predominant peaks observed at 4.2 K. The observed PL originates from suppressed dispersion in graphene at a shifted saddle point 0.525(M + K) of the Brillouin zone (BZ). The details of this are explained fully in our previous paper[28]. Here we focus on the dynamical behaviour of these two peaks, which blueshift with increasing temperature due to the negative thermal expansion coefficient of graphene[29–31], these emissions have not been observed in ordinary graphene or GQDs, or GO, given the broad luminescence[13,19–21]. The shape of the P1 peak is asymmetric due to a phonon replica of its excitonic transition with a phonon energy shift of ~4 meV[28], and it was fitted by two Gaussian peaks, peak P2, however, exhibited emission characteristic of a single peak (Supplementary Fig. 1). Note that the intensities of the P1 and P2 peaks show an opposing trend as shown in Fig. 1a, that is, the intensity of the P1 peak becomes broad and intense with increasing temperature. Whereas that of the P2 peak decreases linearly. Inset of Fig. 1b shows the deduced integrated PL intensity

[1]Department of Chemistry, College of Natural Science, Ulsan National Institute of Science and Technology (UNIST), Ulsan 44919, Korea. [2]Clarendon Laboratory, Department of Physics, University of Oxford, Parks Road, Oxford OX1 3PU, UK. [3]Beamline Division, Pohang Accelerator Laboratory, Pohang 37673, Korea. ✉email: ysinpark@unist.ac.kr; cchwang@postech.ac.kr

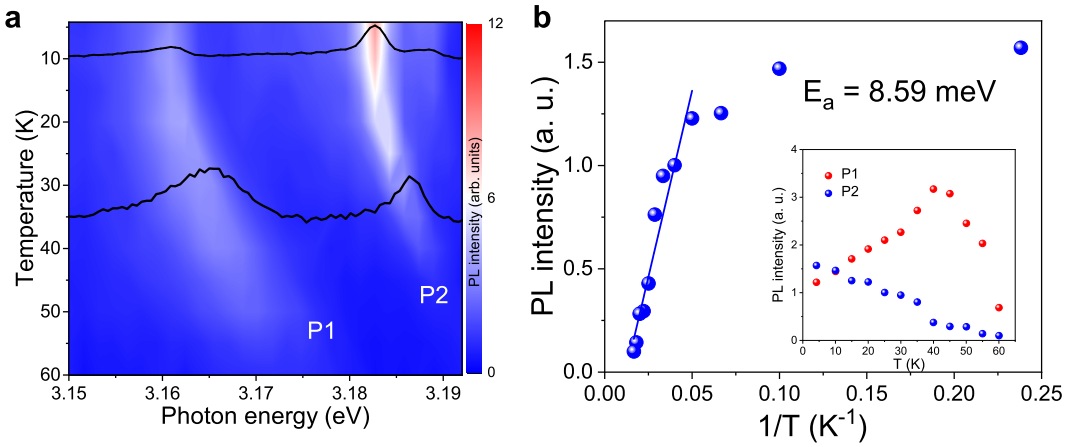

Fig. 1 Temperature-dependent micro-photoluminescence. a Temperature-dependent PL spectral mapping from graphene. Upper and bottom insets depict the PL spectra taken at 4.2 and 35 K, respectively. **b** The Arrhenius plot of the P2 emission. Inset depicts the integrated PL intensity of the P1 and P2 emission peaks as a function of temperature. All intensities are deduced by Gaussian fitting as shown in Supplementary Fig. 1.

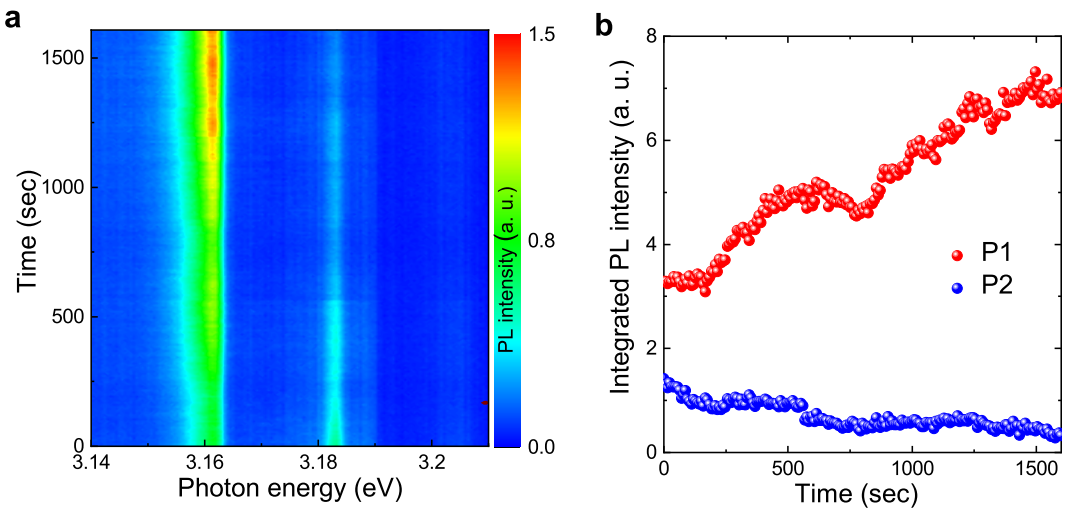

Fig. 2 Temporal variation photoluminescence. a Temporal variation of the PL spectra measured at 4.2 K. **b** The integrated PL intensity as a function of time. The red and blue dots relate to emission from P1 and P2, respectively. The peak intensity was extracted by Gaussian fitting.

of these peaks. As we expected, the intensity of the P2 peak decreases linearly with increasing temperature, whereas that of P1 increases up to ~45 K and then decreases rapidly as the temperature is increased further. The decrease in the intensity with temperature can be understood by ionization of the exciton, however, the increase in the intensity seen for P1 is difficult to explain. The PL intensity (I) as a function of temperature (T) can be expressed as $I = A \exp(-E_a/k_B T)$, where A is a constant, and k_B is the Boltzmann constant. The exciton activation energy (E_a) of P2 was estimated to be 8.59 meV by the Arrhenius plot shown in Fig. 1b.

Figure 2a shows the long-term temporal variation of the PL emission measured at 4.2 K. Consecutive PL spectra at 8 s time-intervals were collected from the graphene sample. Note that apart from the P1 and P2 peaks, the intensities of all other peaks such as that near 3.189 eV etc., which have very weak intensity, keep their original values for a long time. However, the overall intensity of the P1 peak increases with increasing time, while that of P2 decreases. All spectra were fitted by using Gaussian function (Supplementary Fig. 2). The emission intensities of the P1 and P2 peaks change in opposition to each other, that is, the temporal variation of one peak seems to be compensated by that of the other keeping its spectral position and FWHM (Supplementary Fig. 2) for a long time.

Figure 2b shows the integrated PL intensity variation for specific peaks as a function of time. The intensity of the P1 peak increases with time, while that of P2 deceases, which suggests that the carriers are transferred from the states responsible for P2 to those of P1. This behaviour is related to the compensation of the P1 and P2 peaks by each other by moving the exciton from P2 to P1 because the electronic band dispersion of the P1 and P2 arises from the same valence band[28]. In temperature-dependent PL, we need to consider thermal effects with increasing temperature.

Temperature-dependent TRPL

The carrier decay time was characterized by measuring the TRPL. Figure 3 shows the TRPL curves of the P1 and P2 peaks measured at 4.2 K. The decay curves exhibit a single-exponential decay, as shown in the black and red solid lines for the P1 and P2 peaks, respectively. The decay dynamics can be modelled by the following coupled differential equations[32–34].

$$-\frac{dn_f}{dt} = An_f + Bn_f^2 + Cn_f^3 \quad (1)$$

$$-\frac{dn_x}{dt} = k_x n_x \quad (2)$$

where the A arises from trap-assisted recombination due to Shockley–Read–Hall, B is the radiative bimolecular free carrier recombination rate and C is the non-radiative Auger recombination rate, and the Auger contribution is negligible at low temperatures and at all but the highest densities used. The excitonic decay expressed, by Eq. (2), can also be significant at low temperature. Here we assume the exciton density (n_x) and the free carrier decay (n_f) are independent of each other. Only A, B and k_x describe radiative recombination and all other parameters are assumed non-radiative. These equations produce good fits to the data as shown in the blue curves in Fig. 3a. The decay time of the P1 peak is 1.488 ns, which is similar to that of GQDs reported by Xu et al[35]. Although the PL and TRPL of GQDs depend on the excitation wavelength[13,21,36], the 266 nm wavelength excitation used this work is the most efficient for producing emission from the intrinsic state of graphene QDs[13]. The decay time for the P2 peak is, however, ~150 ps, which is very short compared to that of the P1 peak and is therefore impossible to measure accurately as it is almost at the resolution limit of the system. The measured decay time does not imply a direct radiative lifetime for the carriers, that is, the measured PL decay time produces an effective lifetime (τ_{eff}) including radiative (τ_r) and non-radiative lifetimes (τ_{nr}) expressed as $\tau_{eff}^{-1} = \tau_r^{-1} + \tau_{nr}^{-1}$. Since the later can only increase with temperature, which means that the non-radiative rate is significantly smaller than the radiative rate. We can thus safely conclude that the non-radiative decay rates are slower than the radiative ones at low temperatures.

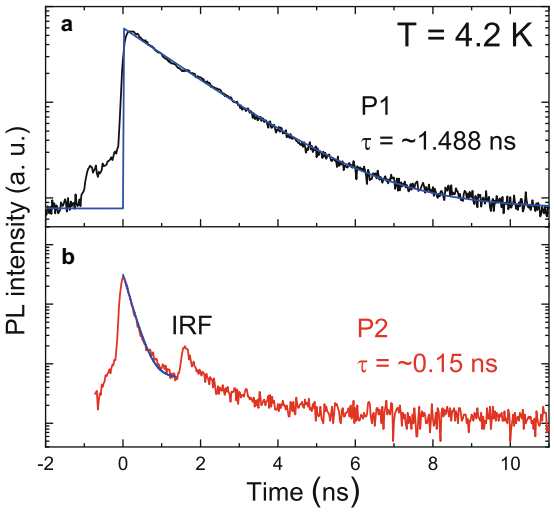

Fig. 3 Time-resolved photoluminescence. a Time-solved PL of the P1 (black solid line) and P2 (red solid line) emission peaks measured at 4.2 K. The blue solid lines are fitted. The excitation power is 2 mW. **b** The shoulder near 1.6 ns is due to the instrument response function (IRF) caused by electron reflections in the system.

The excitation power-dependent TRPL spectra for the P1 peak were shown (Supplementary Fig. 3). The decay decreases slowly with increasing excitation power. As shown in the inset, although the decay time decreases, it only changes by 0.084 ns due to the small but increasing Auger recombination rate. The trapping rate, however, remains almost constant (Supplementary Fig. 3). Note that the Auger recombination rate is independent of the energy gap in many indirect semiconductors, while it decreases exponentially in direct gap semiconductors with an energy gap of less than ~1 eV[37]. The transition energy for the emission from the graphene used here is at ~3.16 eV, which originates from the 0.525(M + K) point of the BZ[28], the actual band gap of graphene is zero.

The inset in Fig. 4a presents a temperature-dependent TRPL mapping of the P1 peak decay at an excitation power of 2 mW. The decay dynamics of the P1 peak remain almost constant or increase slightly up to about ~50 K and then decrease rapidly as the temperature is increased further. The original fitting curves are shown (Supplementary Fig. 4). The PL decay times obtained from single-exponential fits using Eqs. (1) and (2) above as a function of temperature are shown in Fig. 4a. The decay times are almost constant up to ~50 K and then rapidly decrease at higher temperatures. Here, we notice that the initial exciton density of the graphene on the Cu surface decreases monotonically due to the thermal ionization of excitons, whereas the carrier trapping rate increases exponentially with increasing temperature (Fig. 4b). So we can deduce that the carrier dynamics are related to the carrier trapping rate.

Another parameter affecting the decay mechanism is the Auger recombination rate. Theoretically, the Auger recombination rate increases slowly with increasing temperature, corresponding to an indirect Auger recombination process[38–40]. However, the Auger recombination rate is almost constant up to ~45 K and its contribution to the dynamics is almost negligible, and then increases rapidly with a further increase in temperature (Supplementary Fig. 4), which matches well with the excitonic decay time shown in Fig. 4a, albeit with a small contribution to the total decay of 0.22% at 4.2 K and 2.1% at 65 K. It is clear that the excitons are

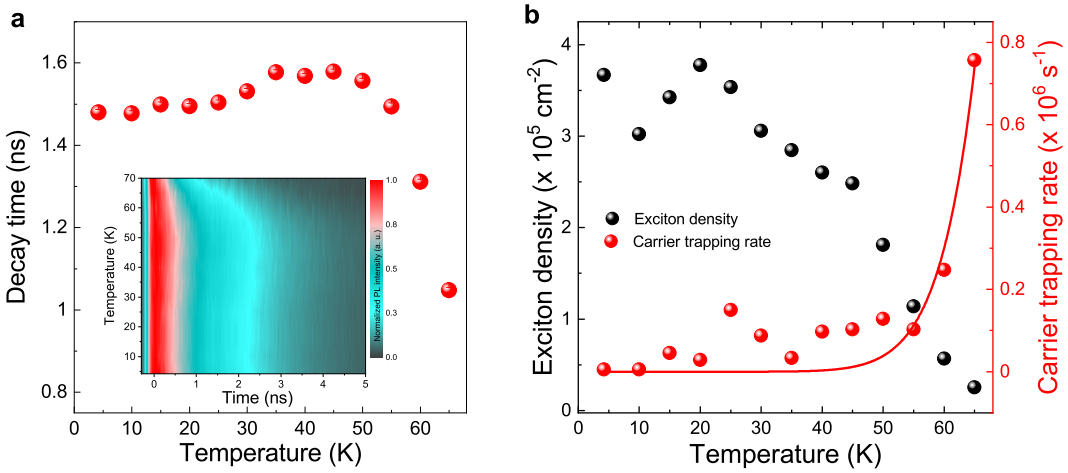

Fig. 4 Temperature-dependent time-resolved photoluminescence. a Decay time of the P1 emission peak as a function of temperature. Inset depicts the temperature-dependent time-resolved PL of the P1 emission peak measured at excitation power of 2 mW. We used a power that was as low as possible to avoid thermal effects. **b** Initial exciton density and carrier trapping rate, which is related to free carrier density n_f, as a function of temperature.

trapped in the low-temperature regime and then become active in the 2D plane as the temperature increases above ~50 K.

In conclusion, the carrier dynamics of the excitonic emission from a monolayer graphene grown on a Cu(111) surface was characterized by temperature and TRPL. The intensity variation of these two peaks with temperature shows an opposing trend, that is, the intensity of the ~3.18 eV peak decreases linearly with increasing temperature, whereas that of the ~3.16 eV peak increases up to ~45 K and then decreases rapidly. The temporal variation of the PL shows that these two peaks are related to each other and compensate the total intensity. The carrier recombination dynamics are mainly dominated by carrier trapping and Auger recombination as the temperature increases.

METHODS

Synthesis of graphene

A monolayer of graphene was synthesized on a single crystal Cu(111) substrate in a hot quartz tube. The Cu(111) was introduced in the middle of the horizontal tube, and then the tube was evacuated, back filled with hydrogen (H_2, 100 sccm) and argon (Ar, 200 sccm) to remove the residual air completely from the tube. The native Cu oxide layer was removed by pre-heating at 1050 °C for 30 min under the H_2 and Ar ambient. More detailed growth condition can be found in ref. [28].

Optical characterization

A frequency-tripled femtosecond Ti:sapphire laser (100 fs pulses at 76 MHz) operating at 266 nm was used to excite the graphene using a micro-PL experimental system. The sample was mounted in a continuous-flow helium cryostat, allowing the temperature to be controlled accurately from 4.2 K to room temperature. A 36× reflecting objective was held by a sub-micron precision piezoelectric stage above the cryostat and used to focus the incident laser beam to a spot size of ~1.2 μm^2 and to collect the resulting luminescence. The luminescence was then directed to a spectrometer with a spectral resolution of ~700 μeV. The signal was finally detected using a cooled charge-coupled device detector. All the PL spectra were obtained using a 0.3 m focal length spectrometer with a 1200 g/mm grating. The TRPL measurements were carried out using the same experimental set up as above, but the dispersed PL was reflected towards a photomultiplier connected to a commercial photon counting system (Becker&Hickl SPC-130), with a time resolution of ~130 ps. Measurements of the lifetimes of the confined states were then carried out over a range of excitation power densities.

DATA AVAILABILITY

The data from this study are available from the corresponding author upon reasonable request.

Received: 19 March 2021; Accepted: 1 July 2021;
Published online: 29 July 2021

REFERENCES

1. Geim, A. K. Graphene: status and prospects. *Science* **324**, 1530–1534 (2009).
2. Geim, A. K. & Novoselov, K. S. The rise of graphene. *Nart. Mater.* **6**, 183–191 (2007).
3. Novoselov, K. S. et al. Electric field effect in atomically thin carbon films. *Science* **306**, 666–669 (2004).
4. Mooradian, A. Photoluminescence of metals. *Phys. Rev. Lett.* **22**, 185–187 (1969).
5. Mueller, T., Xia, F. & Avouris, P. Graphene photodetectors for high-speed optical communications. *Nat. Photonics* **4**, 297–301 (2010).
6. Gan, X. et al. Chip-integrated ultrafast graphene photodetector with high responsivity. *Nat. Photonics* **7**, 883–887 (2013).
7. Koppens, F. H. L. et al. Photodetectors based on graphene, other two-dimensional materials and hybrid systems. *Nat. Nanotechnol.* **9**, 780–793 (2014).
8. Ding, Y. et al. Ultra-compact integrated graphene plasmonic photodetector with bandwidth above 110 GHz. *Nanophotonics* **9**, 317–325 (2018).
9. Ue, G. O. Y. et al. Graphene-based dual-mode modulators. *Opt. Express* **28**, 18456–18471 (2020).
10. Luo, S., Wang, Y., Tong, X. & Wang, Z. Graphene-based optical modulators. *Nanoscale Res. Lett.* **10**, 199 (2015).
11. Wang, H., Nezich, D., Kong, J. & Palacios, T. Graphene frequency multipliers. *IEEE Electron Device Lett.* **30**, 547–549 (2009).
12. Chen, C. et al. Graphene mechanical oscillators with tunable frequency. *Nat. Nanotechnol.* **8**, 923–927 (2013).
13. Liu, F. et al. Facile synthetic method for pristine graphene quantum dots and graphene oxide quantum dots: Origin of blue and green luminescence. *Adv. Mater.* **25**, 3657–3662 (2013).
14. Facure, M. H. M., Schneider, R., Mercante, L. A. & Correa, D. S. A review on graphene quantum dots and their nanocomposites: From laboratory synthesis towards agricultural and environmental applications. *Environ. Sci. Nano* **7**, 3710–3734 (2020).
15. Yoon, H. et al. Blue graphene quantum dots with high color purity by controlling subdomain formation for light-emitting devices. *ACS Appl. Nano Mater.* **3**, 6469–6477 (2020).
16. Song, S. H. et al. Size and pH dependent photoluminescence of graphene quantum dots with low oxygen content. *RSC Adv.* **6**, 97990–97994 (2016).
17. Jin, S. H., Kim, D. H., Jun, G. H., Hong, S. H. & Jeon, S. Tuning the photoluminescence of graphene quantum dots through the charge transfer effect of functional groups. *ACS Nano* **7**, 1239–1245 (2013).
18. Essig, S. et al. Phonon-assisted electroluminescence from metallic carbon nanotubes and graphene. *Nano Lett.* **10**, 1589–1594 (2010).
19. Kim, S. et al. Anomalous behaviors of visible luminescence from graphene quantum dots: interplay between size and shape. *ACS Nano* **6**, 8203–8208 (2012).
20. Shen, J., Zhu, Y., Chen, C., Yang, X. & Li, C. Facile preparation and upconversion luminescence of graphene quantum dots. *Chem. Commun.* **47**, 2580–2582 (2011).
21. Pan, D., Zhang, J., Li, Z. & Wu, M. Hydrothermal route for cutting graphene sheets into blue-luminescent graphene quantum dots. *Adv. Mater.* **22**, 734–738 (2010).
22. Johansson, P., Xu, H. & Kall, M. Surface-enhanced Raman scattering and fluorescence near metal nanoparticles. *Phys. Rev. B* **72**, 035427 (2005).
23. Senkovskiy, B. V. et al. Making graphene nanoribbons photoluminescent. *Nano Lett.* **17**, 4029–4037 (2017).
24. Ma, C. et al. Engineering edge states of graphene nanoribbons for narrow-band photoluminescence. *ACS Nano* **14**, 5090–5098 (2020).
25. Pavel, V. F., Dmitry, V. R., Alexander, I. C., Ekaterina, A. O. & Elena, D. O. Excitonic photoluminescence of ultra-narrow 7-armchair graphene nanoribbons grown by a new bottom-up approach on a Ni substrate under low vacuum. *J. Phys. Chem. C.* **124**, 25984–25991 (2020).
26. Chen, Y. C. et al. Tuning the band gap of graphene nanoribbons synthesized from molecular precursors. *ACS Nano* **7**, 6123–6128 (2013).
27. Wang, J., Zhao, R., Yang, M., Liu, Z. & Liu, Z. Inverse relationship between carrier mobility and bandgap in graphene. *J. Chem. Phys.* **138**, 084701 (2013).
28. Park, Y. et al. Two-dimensional excitonic photoluminescence in graphene on a Cu surface. *ACS Nano* **11**, 3207–3212 (2017).
29. Yoon, D., Son, Y.-W. & Cheong, H. Negative thermal expansion coefficient of graphene measured by Raman spectroscopy. *Nano Lett.* **11**, 3227–3231 (2011).
30. Zakharchenko, K. V., Katsnelson, M. I. & Fasolino, A. Finite temperature lattice properties of graphene beyond the quasiharmonic approximation. *Phys. Rev. Lett.* **102**, 046808 (2009).
31. Jiang, J.-W., Wang, J.-S. & Li, B. Thermal expansion in single-walled carbon nanotubes and graphene: nonequilibrium Green's function approach. *Phys. Rev. B* **80**, 205429 (2009).
32. Wehrenfennig, C., Eperon, G. E., Johnston, M. B., Snaith, H. J. & Herz, L. M. High charge carrier mobilities and lifetimes in organolead trihalide perovskites. *Adv. Mater.* **26**, 1584–1589 (2014).
33. Xing, G. et al. Transcending the slow bimolecular recombination in lead-halide perovskites for electroluminescence. *Nat. Commun.* **8**, 14558 (2017).
34. Yasuda, H. & Kanemitsu, Y. Dynamics of nonlinear blue photoluminescence and Auger recombination in $SrTiO_3$. *Phys. Rev. B* **77**, 193202 (2008).
35. Xu, Q. et al. Single-particle spectroscopic measurements of fluorescent graphene quantum dots. *ACS Nano* **7**, 10654–10661 (2013).
36. Liu, R., Wu, D. & Feng, X. Bottom-up fabrication of photoluminescent graphene quantum dots with uniform morphology. *J. Am. Chem. Soc.* **133**, 15221–15223 (2011).
37. Bulashevich, K. A. & Karpov, S. Y. Is Auger recombination responsible for the efficiency rollover in III-nitride light-emitting diodes? *Phys. Status Solidi (c.)* **5**, 2066–2069 (2008).
38. Kioupakis, E., Yan, Q., Steiauf, D., Van, D. & Walle, C. G. Temperature and carrier-density dependence of Auger and radiative recombination in nitride optoelectronic devices. *N. J. Phys.* **15**, 125006 (2013).
39. Chow, W. W. Modeling of temperature and excitation dependences of efficiency in an InGaN light-emitting diode. *Opt. Express* **22**, 1413 (2014).
40. Ryu, H.-Y., Ryu, G.-H., Onwukaeme, C. & Ma, B. Temperature dependence of the Auger recombination coefficient in InGaN/GaN multiple-quantum-well light-emitting diodes. *Opt. Express* **28**, 27459 (2020).

ACKNOWLEDGEMENTS

This work was supported by the National Research Foundation of Korea (NRF) grant funded by the Korea government (MSIT) (2018R1D1A1B07043676 and 2021R1A2C1006113), and the SRC Center for Topological Matter (2018R1A5A6075964).

AUTHOR CONTRIBUTIONS

Y.P. performed the PL measurement and wrote the manuscript. G.Y. performed the analysis the TRPL. C.C.H. synthesised and supervised the project. R.A.T. supervised the all optical experiments and edited the paper. Y.P. and G.Y. contributed equally to this work.

COMPETING INTERESTS

The authors declare no competing interests.

ADDITIONAL INFORMATION

Supplementary information The online version contains supplementary material available at https://doi.org/10.1038/s41699-021-00252-x.

Correspondence and requests for materials should be addressed to Y.P. or C.C.H.